In-situ Investigations on Structural Evolutions during the Facile Synthesis of Cubic α-MoC_{1-x} Catalysts

Xingtao Sun[a,b], Jiafeng Yu[a,*], Shuo Cao[a,c], Anna Zimina[d,e], Bidyut Bikash Sarma[d,e], Jan-Dierk Grunwaldt[e,d], Hengyong Xu[a], Shiyan Li[a,b], Yuefeng Liu[a,*], Jian Sun[a,*]

[a]Dalian Institute of Chemical Physics, Chinese Academy of Sciences, Zhongshan Road 457, Dalian 116023, China

[b]University of Chinese Academy of Sciences, Beijing 100049, China

[c]College of Chemical Engineering, Sichuan University, Chengdu 610065, China

[d]Institute of Catalysis Research and Technology, Karlsruhe Institute of Technology, 76344 Eggenstein-Leopoldshafen, Germany

[e]Institute for Chemical Technology and Polymer Chemistry, Karlsruhe Institute of Technology, 76131 Engesserstraße 20, Karlsruhe, Germany

Corresponding authors: yujf@dicp.ac.cn; yuefeng.liu@dicp.ac.cn; sunj@dicp.ac.cn

Abstract

Cubic α-phase molybdenum carbides (α-MoC_{1-x}) exhibit great potential in hydrogen production at low temperatures due to their excellent activity in water dissociation. However, the design strategies of α-MoC_{1-x} is severely restricted by the harsh synthesis conditions, which involves multi-steps ammonification and carburization processes or the utilization of significant amount of noble metals. Herein, high purity α-MoC_{1-x} synthesis in a one-step carburization process was achieved with the assistance of trace amount of Rh (0.02%) as a promoter. The structural evolution of Mo species during phase transition was monitored *via* qualitative and quantitative analysis by *in-situ* X-ray diffraction (XRD) and *in-situ* X-ray absorption spectroscopy (XAS), respectively. In addition, *in-situ* transmission electron microscopy (TEM) was used to follow the changes in visual. We found that the reduction of MoO_3 to cubic oxygen-deficient Mo oxide (MoO_x) that started at a low temperature of about 300°C were vital to the following carbon atoms insertion and transformation to α-MoC_{1-x}. That is because the slow process of lattice oxygen removal and subsequent formation of vacancies was essential in phase shrink from monoclinic to cubic, making the carburization follow the topological transformation. The systematic analysis of the relationship between the reduction behavior and the structural evolution pave the way for a feasible strategy for facile synthesis of the α-MoC_{1-x}, and *in-situ* characterizations shed light on controlling the phase transformation during carburization.

1. Introduction

Transition metal carbides (TMCs), a group of important catalytic materials, have attracted extensive attention due to their unique physical and chemical properties. Molybdenum carbide is one of them with a broad *d*-band structure and exhibits similar catalytic behavior to Pt due to the hybridization of the *d*-orbital of Mo and *s*- and *p*-orbital of carbon[1], making them widely used in reactions that are dominated by noble metals, such as water-gas shift reaction[2,3], ammonia decomposition[4], CO_2 hydrogenation[5,6], methane reforming[7,8] and electro-catalytic hydrogen production[9-11]. The catalytic behavior of molybdenum carbides is vitally interrelated with their crystal structure and configurations. The face-centered cubic (FCC) α-MoC_{1-x} with an ABCABC stacking sequence[12] showed higher activity in the activation of water at low temperature[3,13, 14] in comparison to hexagonal β-Mo_2C with an ABAB packing of the metal planes structure. Synergetic interaction *via* different active sites on α and β phase Mo carbides in dual-phase MoC_x composites was also observed[15]. Given this, efforts on engineering crystal phase, especially metastable cubic α-MoC_{1-x}, during carburization with environmentally-friendly and cost-effective process at moderate conditions are desired.

State of the art synthesis of molybdenum carbide involves temperature-programmed carburization (TPC) process[16], where an oxide precursor, typically MoO_3, is treated under mixtures of hydrocarbons and hydrogen. Generally, hexagonal β-Mo_2C can be synthesized by TPC at 700°C in 20% CH_4/H_2[17], while the formation of metastable α-MoC_{1-x} is much more challenging than the stable β phase and needs more

complex procedures. Therefore, the regulation of the crystalline phases during TPC has been extensively investigated *via* tuning multi-parameters. Usually, an extra temperature-programmed ammonification (TPA) in a stream of pure NH_3 is necessary before TPC for high purity α-MoC_{1-x} synthesis, because an intermediate phase (Mo_2N) with a cubic phase will be first formed during TPA, making the subsequent carburization change from a non-topological route for β-Mo_2C into a topological one for α-MoC_{1-x}[18,19]. However, TPA is an energy-demanding process with requirement of high precautionary measures and corrosion resistance of reactor[20,21]. In addition, formation of the cubic phase was observed in the presence of long chain hydrocarbons[22-24] but always suffered from the coke deposition of carbon source cracking[25]. An alternative approach to generate the cubic α-MoC_{1-x} is from carbon nanotubes or nanofibers support as carbon source, but Mo loading was limited to as low as 7.5 wt.%[26,27]. High-pressure treatment before carburization induces crystallographic orientation of MoO_3 precursor to cubic Mo carbides[28]. Alternatively, an amine-based molybdenum oxide precursor is also beneficial to this process[29]. The addition of high loading of Au, Pd and Pt were shown to be able to promote the formation of α-MoC_{1-x}[13,14,18]. However, the promotion is less efficient when lowering the amount of noble metals[30]. In comparison, trace amounts of Rh addition as a promoter is a good alternative for one-step synthesis of α-MoC_{1-x} catalysts without ammonification from our previous work[31], but the phase transformation route and the formation of key intermediates during carburization were unclear. It has been reported that cubic MoO_yC_x intermediate accompanied with MoO_2 formed after 3wt.% Au addition and

then subsequently converted into α-MoC_{1-x} at high temperature[13]. It is also proposed that the cubic structure templates, such as molybdenum oxycarbide[19] or oxyhydride[32], were necessary for the formation of α-MoC_{1-x}[33,34], while the monoclinic MoO_2 phase will only lead to β phase[35]. In contrast, it was also reported that α-MoC_{1-x} can be formed from a variety of Mo oxides using heptane or toluene as the carburizing agent without observation of any oxycarbide or oxyhydrate precursors[23]. However, the structural evolution and the reaction pathway during TPC are still unclear, let alone the essential factors of controlling and regulating the carburization process. Therefore, *in-situ* characterizations of the carburization process in the aspect of phase transition, intermediate components, chemical reactions and structural evolution at the atomic level are highly desired, aiming at establishing a multi-parameter toolbox for fine-tuning of the carburization process and crystalline structure.

Herein, the carburization conditions, evolution of the crystal structural evolution and catalytic performance in water-gas shift (WGS) reaction were investigated over molybdenum carbides. Qualitative and quantitative analyses of crystal phases formed as intermediates during the carburization process were carried out by *in-situ* X-ray diffraction (XRD) and *in-situ* X-ray absorption spectroscopy (XAS), respectively. The evolution of morphology and crystal structure was further monitored by environmental transmission electron microscopy (ETEM). The key factors for inducing the formation of α-MoC_{1-x} structure were identified by the separate stepwise reduction and carburization experiments. The reveal of the carburization process from multiple perspectives will enlighten the reaction pathways and the promoting mechanism of

metals, providing a controlling strategy of TMCs synthesis.

2. Results and discussion

2.1. Catalytic performance of Mo carbides

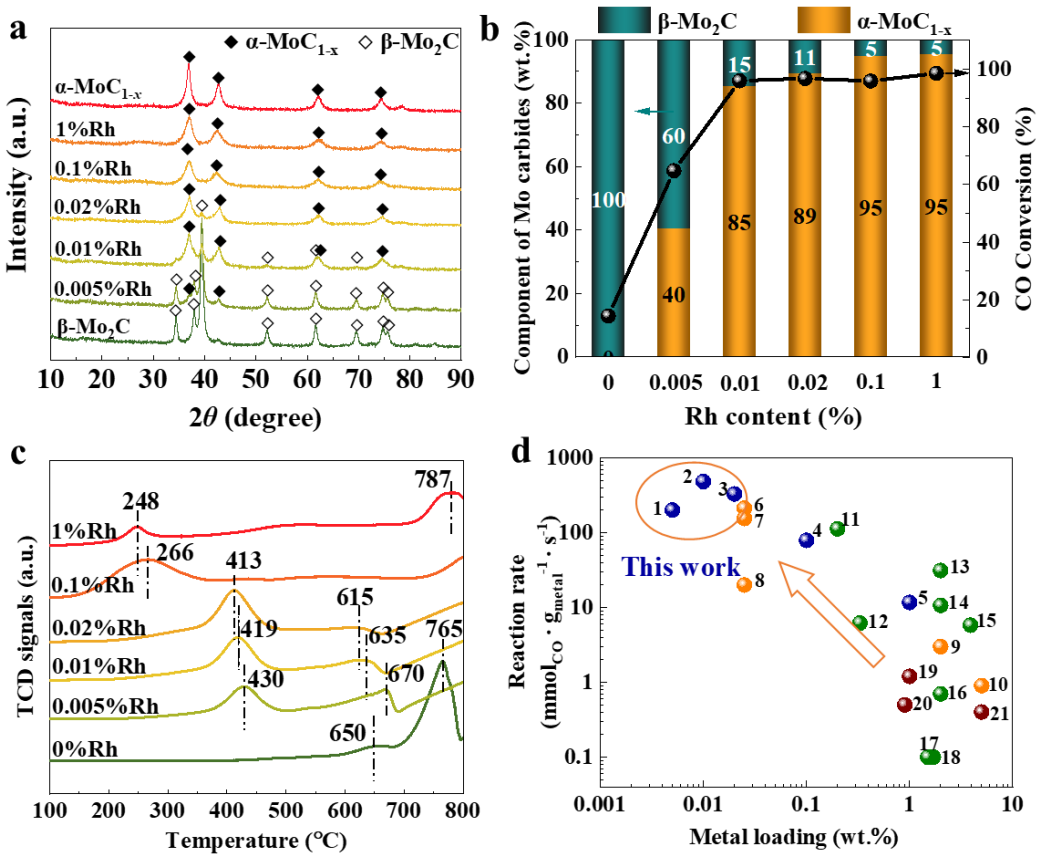

Figure 1. Structure identification and catalytic performance. (a) XRD patterns of standard α-MoC_{1-x} and β-Mo_2C, as well as series Rh/MoC_x samples, which are obtained from the TPC treatment of Rh/MoO_3 with various Rh contents. (b) Fraction of α-MoC_{1-x} in series Rh/MoC_x samples from the linear fitting and their catalytic performance over WGS reaction at 200°C. (c) H_2-TPR results of Rh/MoO_3 samples with various Rh loadings. (d) Comparison of catalytic performance in WGS reaction of Rh/MoC_x catalysts in this work and catalysts in literatures marked with numbers. Blue balls (this work): (1) 0.005%Rh/MoC_x, (2) 0.01%Rh/MoC_x, (3) 0.02%Rh/MoC_x, (4)

0.1%Rh/MoC_x, (5) 1%Rh/MoC_x,); Orange balls (our previous work[31]): (6) 0.025%Rh/MoC_x, (7) 0.025%Pt/MoC_x, (8) 0.025%Au/MoC_x, (9) 2%Rh/MoC_x, (10) 5%Cu/MoC_x; Green balls (noble metals supported on Mo carbides in literatures): (11) 0.2%Pt/α-MoC_{1-x}[36], (12) 0.33%Ir/α-MoC_{1-x}[37], (13) 2%Pt/α-MoC_{1-x}[36], (14) 2%Au/α-MoC_{1-x}[3], (15) 3.9%Pt/β-Mo_2C[38], (16) 2%Au/β-Mo_2C[3], (17) 1.5%Pt/β-Mo_2C[39], (18) 1.7%Pd/β-Mo_2C[39]; Red balls (noble metals supported on oxide supports): (19) 1%Pt-Na/SiO_2[40], (20) 0.9%Au/CeO_2[41], (21) 5%Pt/CeO_2[41].

Standard α-MoC_{1-x} as a reference material was obtained by two-step treatments of MoO_3, including ammonification in pure NH_3 and carburization in 20%CH_4/H_2 at high temperatures (700°C) as reported earlier[18]. Standard β-Mo_2C was synthesized by treating FSP-made MoO_3[31] (without Rh) in 20%CH_4/H_2 atmosphere in a typical one-step TPC process. Here, we simplify the two-step synthesis process for α-MoC_{1-x} into one step by introducing different amounts of Rh on FSP-made MoO_3 by the impregnation method (Figure S1). The crystal structure of synthesized Rh/MoC_x is identified by XRD in Figure 1a. The addition of Rh has a great impact on the crystal phase of Mo carbides during one-step carburization. The proportion of α-MoC_{1-x} significantly increases with increasing Rh loadings, while the β-Mo_2C component decreases correspondingly and finally disappears over 0.1% Rh/MoC_x catalyst. The proportion of α phase in all Mo carbides is roughly evaluated by the intensity ratio of their typical peaks in XRD patterns (Figure S2), which is calibrated through the linear fitting with the weight ratio of standard α-MoC_{1-x} and β-Mo_2C. As shown in Figure 1b, about 85% α-MoC_{1-x} can be created by adding only 0.01 wt.% Rh, while the

enlargement of Rh content by 100 times (1 wt.%) will bring a slight enhancement to 95%. The function of Rh in α-MoC_{1-x} synthesis exceeds those 0.025% Pt and 0.025% Au reported previously by our group[31]. The CO conversion in the WGS reaction exhibits a similar trend with α-MoC_{1-x} content. It is enhanced from 14 to 65% when α-MoC_{1-x} is increased from 0 to 40% and further enhanced to 96% when increasing the proportion of α-MoC_{1-x} to 85%. All of the Rh/MoC_x catalysts with Rh loading above 0.01% exhibit a little higher activity than the two-step synthesized α-MoC_{1-x} standard sample, demonstrating that the presence of a small amount of inactive β-Mo_2C detected in XRD on Rh-catalysts will not affect their catalytic performance (Figure S3). From the H_2-TPR results in Figure 1c, the addition of Rh greatly enhances the MoO_3 reduction. The temperature decreases from 650 to 430℃ with the addition of 0.005% Rh, then further decreases to 245℃ when increasing Rh loading to 1%. The acceleration of reduction might be related to the hydrogen dissociation on Rh and spillover to the MoO_3. Similar results were also observed on Pt and Au as long as increasing the loading to 2 wt.%[13,14]. To evaluate the role of Rh, we summarize the catalytic performance of Rh samples in this work and those reported catalysts with noble metals in Figure 1d and Table S1. The best performance of 484 and 330 $mmol_{CO}\cdot g_{Rh}^{-1}\cdot s^{-1}$ can be achieved over 0.01 and 0.02% Rh/MoC_x catalysts, respectively, exhibiting excellent utilization efficiency of noble metals. The reaction rates are referred to the Rh contents determined by ICP (Table S2) and catalytic tests under kinetic conditions (Figure S4) to underline its role already at low concentrations. This finding opens up a new possibility of simplification of the carburization process in a one-step process with high utilization

efficiency of noble metals.

2.2. Variations of crystal phase during carburization

Qualitative analysis of the crystal phase during the carburization process was realized by *in-situ* XRD measurements, focusing on the revealing of the structural evolution at different stages of TPC. The XRD patterns at the initial stage are MoO_3 in both MoO_3 and 0.02%Rh/MoO_3 samples as shown in Figures 2a and 2c, respectively. Further details are presented in Figures S6 and S7. For the MoO_3 sample, it is unable to be reduced until the temperature reaches as high as 500℃. The reduction of MoO_3 to Mo_4O_{11} and MoO_2 is observed step-by-step at about 500 and 600℃, respectively. Then the carburization occurs rapidly with the conversion from MoO_2 into β-Mo_2C in a short time when the temperature rising from 690 to 700°C (Figure 2b). No sign of α-MoC_{1-x} can be detected during the whole process. However, the TPC process is totally different after addition trace amount of Rh (0.02%) in MoO_3 by impregnation method for 0.02%Rh/MoO_3 sample. The starting reduction temperature of MoO_3 remarkably decreases from 500 to 210°C. MoO_3 is first reduced to Mo_2HO_6 at about 200-300℃, and then the reduction and carburization successively occur in the temperature range from 300 to 560°C, leading to the formation of a cubic phase with typical two reflections but at a relatively large angle (39° and 44°) compared to α-MoC_{1-x} (36.4° and 42.3°). It indicates that the Mo species in this stage is in a cubic structure but with smaller lattice parameters. It might be oxygen-deficient Mo oxides in a cubic structure (named as MoO_x) with a large number of oxygen vacancies created during reduction. With increasing temperature, it will turn into MoO_xC_y when C atoms insert into the

oxygen vacancies accompanied with lattice expansion, which is proposed to be an oxycarbide intermediate of an FCC structure[18] and a transition phase of α-MoC_{1-x}. As a result, the two reflections gradually shift to a lower angle along with the lattice expansion during this process. Subsequently, O atoms in MoO_xC_y are completely substituted by C atoms accompanied by peak shift and intensity increase (Figure 2d), and it finally turns into α-MoC_{1-x} *via* the topological route. The main feature of β-Mo_2C at 39.5° appears at about 700°C, which is derived from the small amount of MoO_2 at 26° as detected during TPC. This is similar to the carburization process of MoO_3, demonstrating that the configuration of intermediates depends on the phase structure of products.

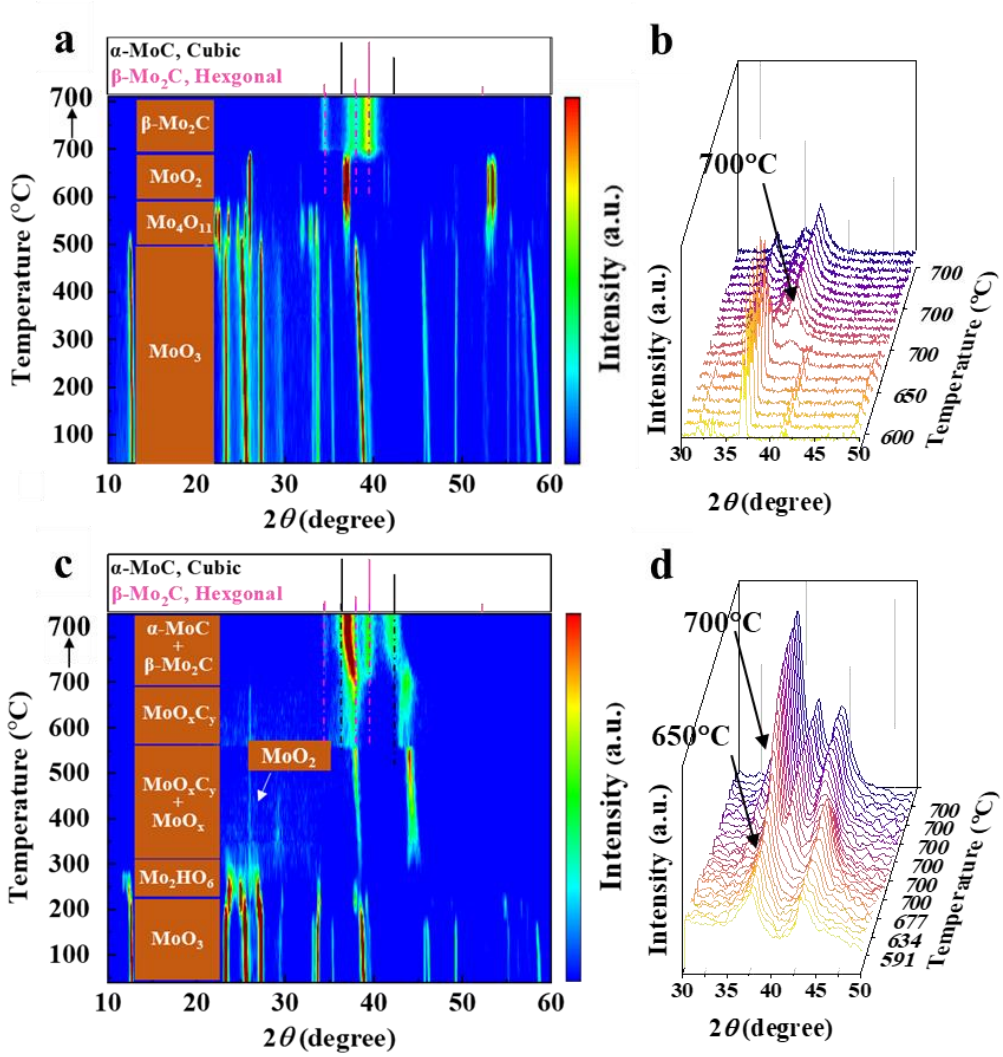

Figure 2. *In-situ* XRD patterns of (a, b) MoO_3 and (c, d) 0.02%Rh/MoO_3 during the TPC process in 20%CH_4/H_2 atmosphere. The dominated phases of Mo species at each stage are listed on the left side of the contour map. The standard diffraction peaks of α-MoC_{1-x} and β-Mo_2C phases are shown on the top, while those of MoO_3, Mo_4O_{11}, MoO_2, Mo_2HO_6, MoO_xC_y are presented in Figure S5.

2.3. Reduction behavior during carburization

From the above XRD analysis, the whole TPC process involves reduction and carburization. Here, we separated these two processes in order to further investigate the function of reduction and carburization without hydrogen. 0.02%Rh/MoO_3 sample was

first reduced at different temperatures in pure H_2 (XH) and further carburized in 20%CH_4/He at 700°C without H_2 (XH-700M). The XRD patterns of the above samples are shown in Figure 3a and 3b, respectively. The MoO_3 phase in the fresh sample turns into Mo_4C_{11} and MoO_2 after carburization in methane atmosphere without hydrogen (700M). During reduction process, MoO_3 can be reduced into MoO_xH_y by hydrogen insertion in the lattice at 200°C and further to MoO_x at 300°C. The MoO_x species has a face center cubic (FCC) structure with a_{cub} = 0.410 nm and is proposed to be the mixed phases of Mo_9O_{26}, $Mo_{13}O_{33}$ and other Mo oxides[34,42]. MoO_x is stable until the reduction temperature reaches 500°C. Then it is suddenly reduced to two different kinds of Mo metal (Figure S8) at a higher temperature. After carburization, the samples pre-reduced at lower temperatures (200-500℃) contain more α-MoC_{1-x}, while those pre-reduced at 600 and 700℃ are dominated by β-Mo_2C. It is worth noting that the MoO_x species with the typical peaks at 39° and 44° can be confirmed to be a key intermediate during α-MoC_{1-x} formation from this experiment since the carbon source is not introduced at the reduction stage. MoO_xC_y species with similar typical peaks can only be formed in the presence of both CH_4 and H_2 as observed in *in-situ* XRD.

The component of Mo carbides in XH-700M samples and the O/Mo ratio obtained from XPS results of the XH samples are related to their reduction temperatures in Figure 3c. After reduction at low temperature (200℃), the partially reduced Mo oxide with O/Mo ratio of 2.8 leads to the formation of a large amount of β-Mo_2C accompanied with α-MoC_{1-x}. The O/Mo ratio decreases with increasing reduction temperatures and keeps unchanged at about 2.2 during 400-500℃. Then the O/Mo ratio suddenly drops

to 0 at higher reduction temperatures (600-700℃). The amount of α-MoC_{1-x} reaches the maximum value during 400-500℃ and seriously decreases with increasing the reduction temperatures. The β-Mo_2C becomes the main component when O is deeply removed at high temperatures. A volcano curve of α-MoC_{1-x} proportion with increasing reduction temperature is observed, indicating that the control of the reduction state is crucial for the phase transformation. Large amount of α-MoC_{1-x} are generated from the carburization of MoO_x (x=2.0-2.5) intermediate phase that formed at a moderate reduction temperature range. Moreover, the effects of MoO_3 precursor and different noble metals on the reduction process are also investigated (Figure S9). The MoO_x species can form during the reduction treatment and keep stable in the temperature range of 300-500℃ for 0.02%Rh/MoO_3-FSP sample, while they are deeply reduced to Mo at 500℃ for 0.02%Rh/MoO_3-CM prepared by calcination method (CM). Once loading the same amount of Pt (0.02%Pt/MoO_3-FSP), phase transfer occurs from cubic MoO_x to monoclinic MoO_2, leading to more β-Mo_2C. The phase transfer can be efficiently inhibited when increasing the Pt loading to 2%. These results demonstrate that both trace amounts of Rh (0.02%) play an important role in stabilizing the MoO_x intermediate phase as the function of 2% Pt, providing a possibility of reducing the utilization of noble metals during the carburization process. Nevertheless, the reduction process is decisive since the carburization will not happen without hydrogen even in the presence of Rh (Figure S10).

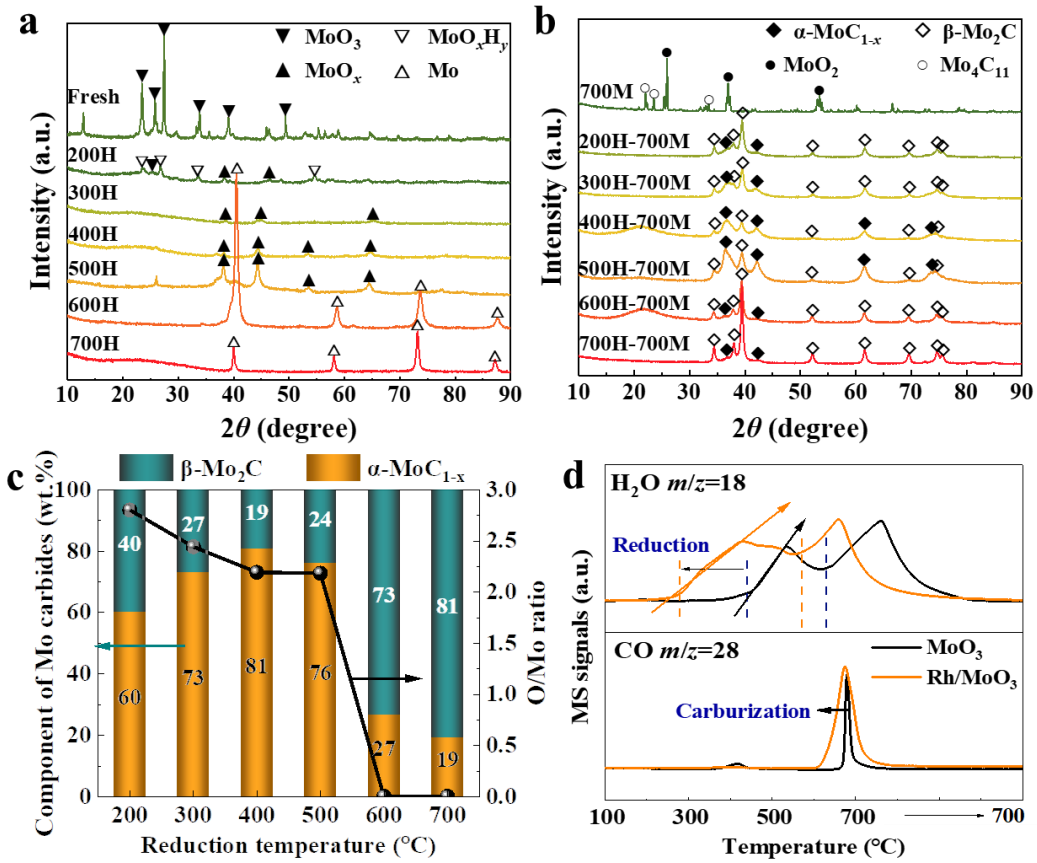

Figure 3. XRD patterns of 0.02%Rh/MoO_3 sample after (a) reduction in pure H_2 and (b) carburization in 20%CH_4/He process without hydrogen. Reduction process: the samples are reduced in hydrogen for 2h at various temperatures and denoted as XH (hydrogen), where X is the reduction temperature. Carburization process without hydrogen: the reduced samples above are further carburized from RT to 700°C and held for 2h, which are denoted as XH-700M (methane). (c) The component of Mo carbides (α-MoC_{1-x} and β-Mo_2C) and O/Mo ratio in 0.02%Rh/MoO_3 sample reduced at different temperatures. (d) The mass spectrometry signal of gas-phase products H_2O (m/z=18) and CO (m/z=28) during carburization (20%CH_4/H_2) in temperature-programmed surface reaction (TPSR) of MoO_3 and Rh/MoO_3 samples. The temperature ramping rate was 5°C/min in all cases.

The temperature-programmed surface reaction (TPSR) experiment was designed to monitor the chemical reactions during the TPC process in 20%CH_4/H_2 (Figure 3d). The production of H_2O appears to be as low as 300℃ and reaches the maximum value between 400 and 500℃ for Rh/MoO_3 sample, while the reduction process occurs at 500℃ for MoO_3. In addition, the reduction rate of MoO_3 is higher than Rh/MoO_3 according to the slope of H_2O signals, because the former starts at a higher temperature. Quick reduction process and high reduction temperature during TPC process will lead to deep reduction and phase transfer. In the low-temperature region, the lattice oxygen is gradually removed accompanied by lattice contraction from orthogonal to cubic phase that driven by the formation of oxygen vacancies. However, the lattice will directly transfer to the more stable monoclinic MoO_2 state if the reduction happens too fast. The carburization process starts earlier (temperature decreasing from 660 to 600℃) and slower for Rh/MoO_3 than MoO_3, generating H_2O and CO simultaneously.

2.4. Variations of phase composition during carburization

The Mo species and their variations were monitored by the X-ray absorption spectroscopy (XAS) technique. It is found that the addition of Rh will not affect the electronic and atomic structure of MoO_3 (Figure S11). The normalized XANES spectra of one-step carburized MoC_x and 0.02%Rh/MoC_x are compared to the reference data of Mo, MoO_2 and MoO_3 (Figure 4a), as well as α-MoC_{1-x} and β-Mo_2C (Figure S12). The Mo oxidation state in both materials is found to be 0.9 and 1.8, which is consistent with those in β-Mo_2C and α-MoC_{1-x}, respectively. The shift of absorption edge (E_0) in XANES spectra can be assumed to be in a linear relation with the oxidation state of Mo

species[3]. The α and β phases in the carburization products of the two samples are also identified by the k^3-weighted Mo K-edge EXAFS spectra in both *k*- and *R*-space compared to the β-Mo_2C and α-MoC_{1-x} reference (Figures S13 and S14), respectively. Two distinguished features marked with blue circles in *k*-space and differences between 4.5 and 4.8 Å in *R*-space can be identified, when compared with the reference samples[43], indicating that the main Mo species in MoC_x and Rh/MoC_x samples are β-Mo_2C and α-MoC_{1-x}, respectively. However, the EXAFS fitting results are unable to distinguish the differences since their structures are similar at short range.

In-situ XAS measurements at Mo K-edge are conducted on MoO_3 and Rh/MoO_3 samples as shown in Figures S15 and S16, respectively. The comparison at different carburization stages is plotted in Figures S17 and S18, respectively. Generally, the carburization process can be divided into three stages, i.e., reduction, stable intermediate state and final phase transition. For MoO_3, a significant reduction can be seen between 481 to 515°C according to the variations of the features of XANES spectra. Then it will go through a phase stable state without any change until 565°C. After that, phase transition happens accompanied by further reduction and finally to β-Mo_2C at 613°C. In comparison, the addition of Rh could promote the reduction in the low-temperature range (300-380°C). A little extent of phase transformation is observed during 380-510°C without any change in Mo valence state. Subsequently, phase transition accompanied by further reduction is also detected from 510°C, but it finally transfers to α-MoC_{1-x} at 600°C.

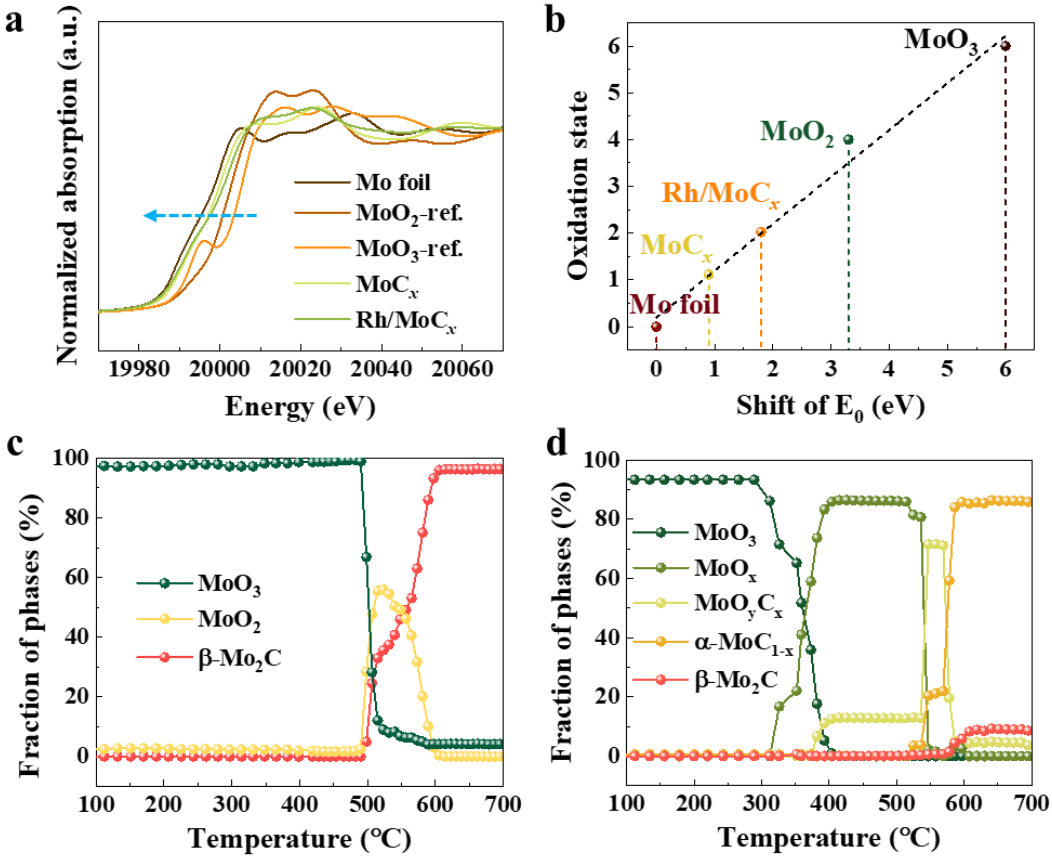

Figure 4. Identification of Mo valence states in the carburization products MoC_x and Rh/MoC_x by (a) normalized Mo K-edge XANES spectra and (b) the relative to Mo^0 position of the absorption edge. The variations of Mo species components during the TPC process according to the LCF results of *in-situ* XANES spectra at Mo K-edge on (c) MoO_3 and (d) Rh/MoO_3 samples. The carburization atmosphere is $20\%CH_4/H_2$, and the temperature ramping rate is 5°C/min. The error bar for LCF is ±5%.

Quantitative analysis was based on the linear combination fitting (LCF) for MoO_3 and Rh/MoO_3 samples, which are shown in Figures 4c and 4d, respectively, aiming at evaluating the extent of transformation among different Mo species along with the carburization process. For MoO_3, the percentage of MoO_2 quickly increases to about 55% at a temperature range of 500-550°C, indicating that the reduction from MoO_3 to

MoO_2 is very fast. Meantime, the carburization occurs since the amount of MoO_2 decreased and β-Mo_2C rapidly reaches 100%. In contrast, after Rh addition, MoO_3 is gradually reduced to MoO_x in a relatively longer period of time with temperature increasing from 300 to 400°C. During this process, about 15% MoO_xC_y forms and then co-exists with 85% MoO_x in a stable state at a broad temperature range from 400-510°C. The carburization is strengthened with a quick phase transformation from MoO_x to MoO_xC_y and further stabilized in a mixture of 85% α-MoC_{1-x} and 10% β-Mo_2C from about 660°C.

2.5. Variations of phase morphology during carburization

Environmental transmission electron microscopy (ETEM) has been used to dynamically monitor the nucleation and growth of the nanocrystal, which allows the investigation of growth mechanism of Mo_2C at an atomic scale[44-47]. The ETEM technique was used to visualize the evolution of promoter phases in Mo substrates from oxides to carbides under carburizing conditions. The morphological variation is observed from solid particles to small fragments as shown in Figure 5a and Figure S19, indicating that pulverization and fragmentation occur during the carburization process from oxides to carbides. FFT patterns of TEM images (Figure S20) and diffraction patterns collected at different temperatures are shown in Figure 5b and Figure 5c, respectively. Those for fresh precursor at 300℃ (300℃-He) and intermediate state at 350℃ are displayed for comparison in Figure S21 and Figure S22, respectively. It can be observed that the crystal structure is unchanged during the gas atmosphere switch from He to 20%CH_4/H_2. Then the structure is gradually deformed with increasing

temperature. At 300℃, the angle between the crystal plane (111) and (101) is 45.1° and the one (200) is not observed due to its large lattice distance, indicating that orthogonal MoO_3 is dominated. At 400℃, the angle between the crystal plane (111) and (200) turns into 52.9°, demonstrating the presence of a cubic structure.

For better understanding of the structural evolution of the phases, we summarize the lattice distance measured from FFT (Figure 5d) and normalized electron diffraction simulated from diffraction patterns (Figure 5e) at various carburization temperatures. From Figure 5d, remarkable shrink in the lattice distance and atom rearrangement in the range of 300 and 400℃ occurs, corresponding to phase transfer from orthogonal MoO_3 to cubic MoO_x. Then three main lattice planes stay stable until 600℃. Finally, the plane with large distance of 3.3 Å disappears, and the other two planes slightly increase and become close to the (111) and (200) planes of α-MoC_{1-x} between 600-700℃. A similar phenomenon is detected from the analysis of diffraction patterns as shown in Figure 5e. The obvious variations between the temperature range of 300-400℃ and 600-700℃ correspond to the large phase transfer of reduction and carburization, respectively. The cubic MoO_x and MoO_xC_y species are intermediate phases during the two processes. The disappearance of the crystal plane (101) during 600-700℃ indicates that Mo oxides were completely carburized to α-MoC_{1-x}. Additionally, continuous particle growth and crystallization are found under carburization conditions at 700℃ (Figure S23). The above evolution of phase morphology is fundamentally consistent with *in-situ* XRD and *in-situ* XAS characterizations. Furthermore, a blank *in-situ* TEM experiment is conducted following the same procedure under 20%CH_4/He without

hydrogen to exclude the effect of a high-temperature environment and identify the decisive reduction condition (Figure S24). We found that the final product is monoclinic MoO_2 rather than Mo carbides, revealing that the carburization was unable to proceed without hydrogen.

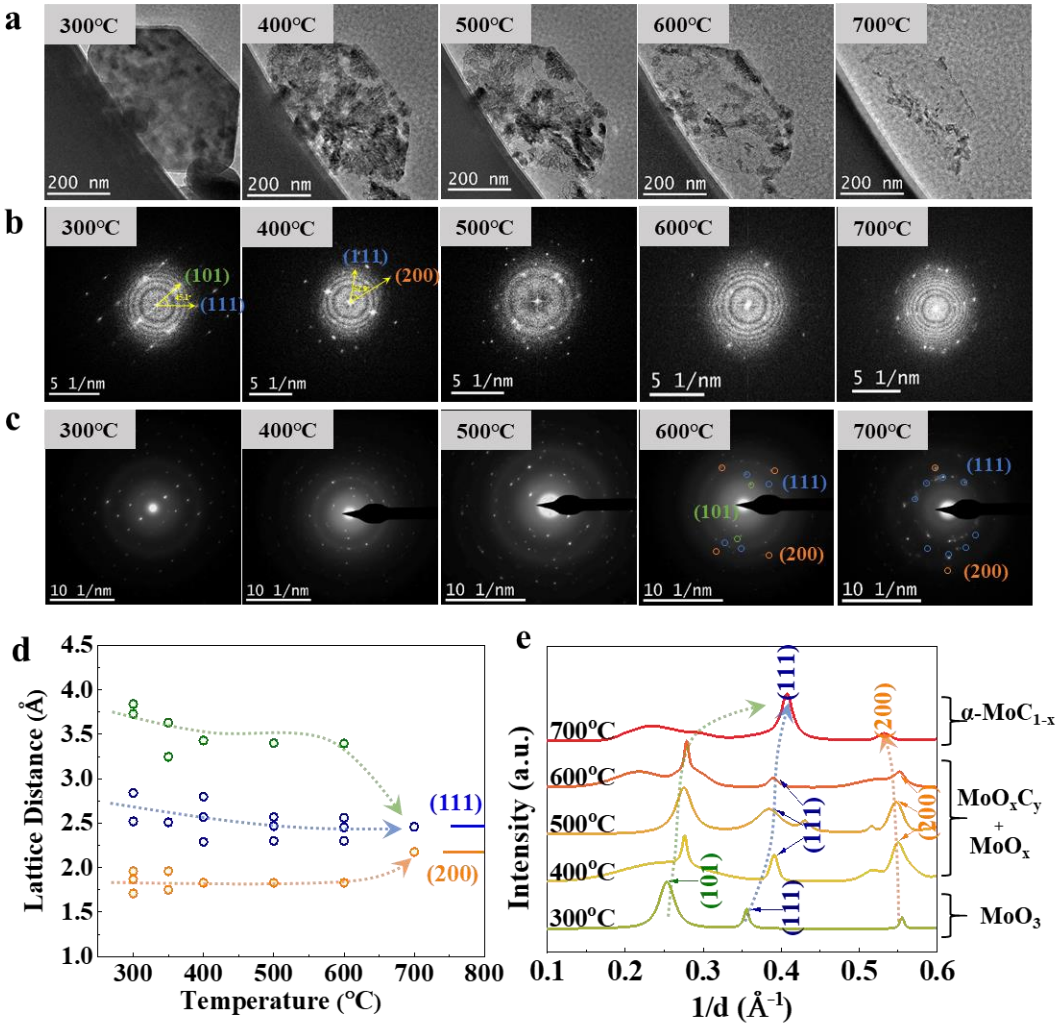

Figure 5. Observation of structural evolution *via* environmental transmission electron microscopy (ETEM). (a) *In-situ* TEM images, (b) Fast Fourier transform (FFT) patterns and (c) electron diffraction patterns for Rh/MoO_3 sample at various carburization temperatures in 20%CH_4/H_2 atmosphere. (d) The changes of lattice distance extracted from FFT patterns with increasing carburization temperature, where the standard

distance of (111) and (200) lattice planes in α-MoC_{1-x} are marked. (e) Normalized electron diffraction radial profiles simulated from the diffraction patterns at different carburization temperatures, showing the variations of crystal planes and the corresponding Mo species during the carburization process.

2.6. Structural evolution during carburization

From the above analysis, we found that the structural evolution during TPC strongly depends on the reduction behavior as illustrated in Figure 6. In the high-temperature reduction pathway (at least 500°C), MoO_3 will be quickly reduced to monocline MoO_2 and transferred to β-Mo_2C *via* a non-topological route. In contrast, if the reduction temperature decreased to as low as 300°C, the carburization can be divided into reduction and carburization processes. During the reduction process, MoO_3 is slowly reduced into MoO_x with a large number of oxygen vacancies, where lattice O atoms are combined with the active H created by promoter Rh sites to generate H_2O. Meantime, the crystal structure is changed from orthogonal to cubic with the lattice shrink. For the carburization process, C atoms from the carbon source (CH_4) first diffuses into the MoO_x lattice and occupied the oxygen vacancies, forming oxy carbides (MoO_xC_y) as intermediates. Then O atoms are gradually reacted with CH_4, accompanied by the carbon substitution and the generation of H_2O and CO. The lattice is slightly expanded by the carbon insertion and finally reaches the α phase structure by the topological route. From the analysis of the two routes, we found that the removal of O atoms and the creation of oxygen vacancies in the reduction process at low temperatures (300-400°C) have great effects on the insertion and substitution of C

atoms and are believed to be the key factor for the structural evolution to cubic α-MoC_{1-x}.

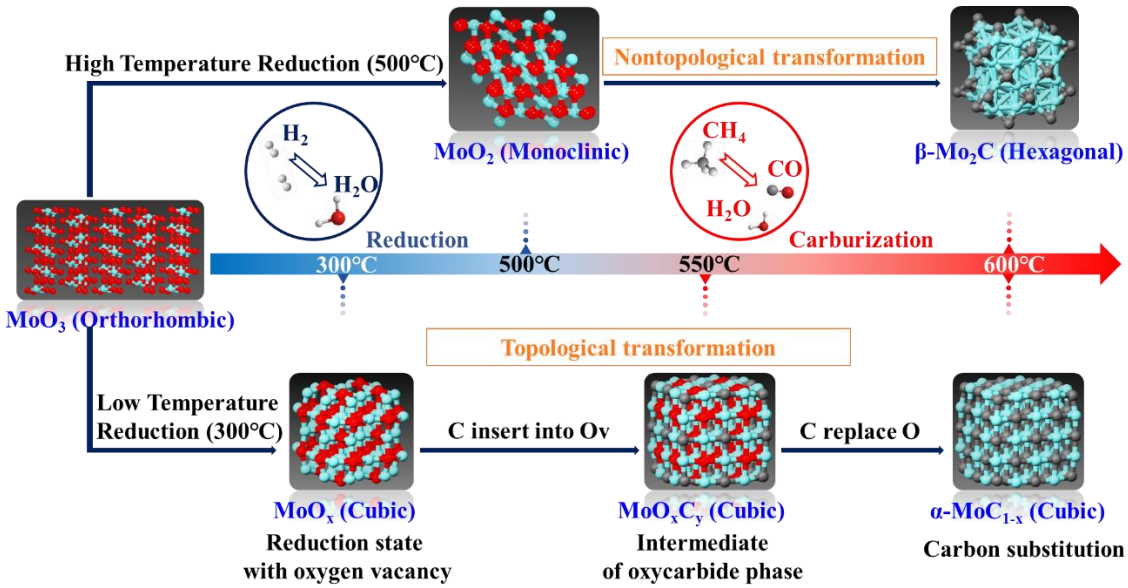

Figure 6. Schematic illustration of the evolution of the various crystalline phases and carburization pathways of MoO_3 with different reduction behaviors during the carburization process.

3. Conclusions

High purity α-MoC_{1-x} was facilely synthesized in a one-step carburization process in the presence of trace amount of Rh (0.02%) as a promoter, which can substitute for ammonification or 2% Pt consumption. The best performance of 484 $mmol_{CO}\cdot g_{Rh}^{-1}\cdot s^{-1}$ in WGS reaction can be achieved, exhibiting excellent utilization efficiency of noble metals compared to those in literatures. The carburization process was systematically studied by a series of *in-situ* techniques (XRD, XAS and TEM) from different aspects (qualitative, quantitative and visualized analysis) under practical conditions. The results reveal that MoO_3 is first reduced to cubic oxygen-deficient Mo oxide (MoO_x) once the reduction started at a temperature of about 300°C, then carbon atoms are able to occupy

the oxygen vacancies to form cubic MoO_xC_y intermediates, which are vital to the further transformation to α-MoC_{1-x} *via* the topological route. The final phase of carbides depends on the primary structure of the initial intermediates and the route of structural evolution during TPC, where slow and stepwise reduction is necessary for the formation of active α-MoC_{1-x}. Revealing the key factor for the structural evolution provides a more facile and universal strategy for the one-step synthesis of α-MoC_{1-x}, which is focusing on the reduction of MoO_3 under mild conditions. The benefit lies in the utilization of minimal amount of noble metal as promoter for the Mo carbides production and controlling phase transformation during the carburization process to resolve the problems of α-MoC_{1-x} preparation.

Acknowledgments

This study was supported by the National Natural Science Foundation of China (22172169, 21972140 and 22172161), the Liaoning Revitalization Talents Program (XLYC1907066 and XLYC1907053) and the Youth Innovation Promotion Association of Chinese Academy of Sciences (2018214 and 2018220). We would like to thank the Institute for Beam Physics and Technology (IBPT-KIT) for the operation of the storage ring, the Karlsruhe Research Accelerator (KARA). We acknowledge the KIT light source for provision of instruments at the CAT-ACT beamline of the Institute of Catalysis Research and Technology (IKFT-KIT). Dr. Yu greatly acknowledges the visiting scholarship from Chinese Academy of Sciences.

References

1. Deng, Y. et al. Molybdenum Carbide: Controlling the Geometric and Electronic

Structure of Noble Metals for the Activation of O-H and C-H Bonds. *Acc. Chem. Res.* **52**, 3372-3383 (2019).

2. Patt, J. et al. Molybdenum carbide catalysts for water-gas shift. *Catal. Lett.* **65**, 193-195 (2000).
3. Yao, S. et al. Atomic-layered Au clusters on α-MoC as catalysts for the low-temperature water-gas shift reaction. *Science* **357**, 389-393 (2017).
4. Zheng, W. et al. Experimental and Theoretical Investigation of Molybdenum Carbide and Nitride as Catalysts for Ammonia Decomposition. *J. Am. Chem. Soc.* **135**, 3458-3464 (2013).
5. Posada-Perez, S. et al. The bending machine: CO2 activation and hydrogenation on delta-MoC(001) and beta-Mo2C(001) surfaces. *PCCP* **16**, 14912-14921 (2014).
6. Posada-Perez, S. et al. Fundamentals of Methanol Synthesis on Metal Carbide Based Catalysts: Activation of CO2 and H2. *Top. Catal.* **58**, 159-173 (2015).
7. Gao, H.F. et al. Simple and large-scale synthesis of beta-phase molybdenum carbides as highly stable catalysts for dry reforming of methane. *Inorganic Chemistry Frontiers* **5**, 90-99 (2018).
8. Christofoletti, T. et al. Methane steam reforming on supported and non-supported molybdenum carbides. *Chem. Eng. J.* **106**, 97-103 (2005).
9. Ma, F.-X. et al. Hierarchical β-Mo2C Nanotubes Organized by Ultrathin Nanosheets as a Highly Efficient Electrocatalyst for Hydrogen Production. *Angew. Chem. Int. Ed.* **54**, 15395-15399 (2015).
10. Yan, Z. et al. MoC-graphite composite as a Pt electrocatalyst support for highly

active methanol oxidation and oxygen reduction reaction. *J. Mater. Chem. A* **2**, 4014-4022 (2014).

11. Chen, W.F. et al. Highly active and durable nanostructured molybdenum carbide electrocatalysts for hydrogen production. *Energy. Environ. Sci.* **6**, 943-951 (2013).
12. Wan, C. et al. Multiple Phases of Molybdenum Carbide as Electrocatalysts for the Hydrogen Evolution Reaction. *Angew. Chem. Int. Ed.* **53**, 6407-6410 (2014).
13. Dong, J. et al. Carbide-Supported Au Catalysts for Water-Gas Shift Reactions: A New Territory for the Strong Metal-Support Interaction Effect. *J. Am. Chem. Soc.* **140**, 13808-13816 (2018).
14. Lin, L. et al. Low-temperature hydrogen production from water and methanol using Pt/alpha-MoC catalysts. *Nature* **544**, 80-83 (2017).
15. Zhang, H. et al. Understanding the synergetic interaction within alpha-MoC/beta-Mo2C heterostructured electrocatalyst. *Journal of Energy Chemistry* **35**, 66-70 (2019).
16. Oyama, S.T. Preparation and Catalytic Properties of Transition Metal Carbides and Nitriles. *Catal. Today* **15**, 179-200 (1992).
17. Sousa, L.A. et al. Hydrotreatment of sunflower oil using supported molybdenum carbide. *Appl. Catal. A* **449**, 105-111 (2012).
18. Jung, K.T. et al. Effects of transition metal addition on the solid-state transformation of molybdenum trioxide to molybdenum carbides. *Chem. Mater.* **16**, 307-314 (2004).
19. Lee, J.S. et al. MOLYBDENUM CARBIDE CATALYSTS .2. TOPOTACTIC

SYNTHESIS OF UNSUPPORTED POWDERS. *J. Catal.* **112**, 44-53 (1988).

20. Fujimoto, S. et al. Stress corrosion cracking of copper in swollen bentonite simulating nuclear waste disposal environment. *Materials and Corrosion-Werkstoffe Und Korrosion* **72**, 333-338 (2021).
21. Shi, W. et al. Anticorrosion Properties of the Low-Temperature Glow Plasma Nitriding Layer on AISI 904L Austenitic Stainless Steel in Hydrofluoric Acid Obtained at Various NH3 Pressures. *Coatings* **10**, 13 (2020).
22. Xiao, T. et al. Effect of carburising agent on the structure of molybdenum carbides. *J. Mater. Chem.* **11**, 3094-3098 (2001).
23. Guzman, H.J. et al. In situ time-resolved X-ray diffraction study of the synthesis of Mo2C with different carburization agents. *Canadian Journal of Chemistry-Revue Canadienne De Chimie* **91**, 573-582 (2013).
24. Mo, T. et al. Effect of carburization protocols on molybdenum carbide synthesis and study on its performance in CO hydrogenation. *Catal. Today* **261**, 101-115 (2016).
25. Xiao, T.C. et al. Preparation of molybdenum carbides using butane and their catalytic performance. *Chem. Mater.* **12**, 3896-3905 (2000).
26. Benjamin Frank, K.F., Frank Girgsdies, Xing Huang, Robert Schlögl, and & Trunschke, A. CNT supported MoxC catalysts: Impact of loading and carburization parameters. *ChemCatChem*, 2296 -2305 (2013).
27. Macedo, L.S. et al. Influence of synthesis method on molybdenum carbide crystal structure and catalytic performance in stearic acid hydrodeoxygenation. *Appl.*

Catal. B **241**, 81-88 (2019).

28. Vitale, G. et al. Low temperature synthesis of cubic molybdenum carbide catalysts via pressure induced crystallographic orientation of MoO3 precursor. *Appl. Catal. A* **400**, 221-229 (2011).
29. Wan, C. et al. Crystal structure and morphology control of molybdenum carbide nanomaterials synthesized from an amine-metal oxide composite. *Chem. Commun.* **49**, 10409-10411 (2013).
30. Ma, Y.F. et al. Low-temperature steam reforming of methanol to produce hydrogen over various metal-doped molybdenum carbide catalysts. *Int. J. Hydrogen Energy* **39**, 258-266 (2014).
31. Sun, X. et al. Controlling phase transfer of molybdenum carbides by various metals for highly efficient hydrogen production. *J. Energy Chem.* **62**, 191-197 (2021).
32. Bouchy, C. et al. On the role of hydrogen during the reduction-carburation of MoO3 into molybdenum oxycarbide. *Journal of Molecular Catalysis a-Chemical* **162**, 317-334 (2000).
33. Delporte, P. et al. PHYSICAL CHARACTERIZATION OF MOLYBDENUM OXYCARBIDE CATALYST - TEM, XRD AND XPS. *Catal. Today* **23**, 251-267 (1995).
34. Bouchy, C. et al. A new route to the metastable FCC molybdenum carbide alpha-MoC1-x. *Chem. Commun.*, 125-126 (2000).
35. Xu, W.Q. et al. Synthesis of alpha-MoC1-x and beta-MoCy Catalysts for CO2 Hydrogenation by Thermal Carburization of Mo-oxide in Hydrocarbon and

Hydrogen Mixtures. *Catal. Lett.* **144**, 1418-1424 (2014).

36. Zhang, X. et al. A stable low-temperature H2-production catalyst by crowding Pt on alpha-MoC. *Nature* **589**, 396-401 (2021).
37. Sun, L. et al. High-Efficiency Water Gas Shift Reaction Catalysis on alpha-MoC Promoted by Single-Atom Ir Species. *ACS Catal.* **11**, 5942-5950 (2021).
38. Schweitzer, N.M. et al. High Activity Carbide Supported Catalysts for Water Gas Shift. *J. Am. Chem. Soc.* **133**, 2378-2381 (2011).
39. Sabnis, K.D. et al. Water-gas shift catalysis over transition metals supported on molybdenum carbide. *J. Catal.* **331**, 162-171 (2015).
40. Zhai, Y. et al. Alkali-Stabilized Pt-OHx Species Catalyze Low-Temperature Water-Gas Shift Reactions. *Science* **329**, 1633-1636 (2010).
41. Fu, Q. et al. Active nonmetallic Au and Pt species on ceria-based water-gas shift catalysts. *Science* **301**, 935-938 (2003).
42. Ma, Y. et al. High-Density and Thermally Stable Palladium Single-Atom Catalysts for Chemoselective Hydrogenations. *Angew. Chem. Int. Ed.* **59**, 21613-21619 (2020).
43. Marquart, W. et al. CO2 Reduction over Mo2C-Based Catalysts. *ACS Catal.* **11**, 1624-1639 (2021).
44. Woehl, T.J. et al. Direct in Situ Determination of the Mechanisms Controlling Nanoparticle Nucleation and Growth. *Acs Nano* **6**, 8599-8610 (2012).
45. Kimura, Y. et al. In Situ Live Observation of Nucleation and Dissolution of Sodium Chlorate Nanoparticles by Transmission Electron Microscopy. *J. Am. Chem. Soc.*

136, 1762-1765 (2014).

46. Qin, F.Y. et al. Anomalous Growth and Coalescence Dynamics of Hybrid Perovskite Nanoparticles Observed by Liquid-Cell Transmission Electron Microscopy. *Acs Nano* **10**, 9787-9793 (2016).
47. Lin, Z.Y. et al. Phase and Facet Control of Molybdenum Carbide Nanosheet Observed by In Situ TEM. *Small* **13**, 1-9 (2017).